

INTERPLANETARY DEPARTURE STAGE NAVIGATION BY MEANS OF LIAISON ORBIT DETERMINATION ARCHITECTURE

Ryan M. McGranaghan*, Jason M. Leonard*, Kohei Fujimoto*, Jeffrey S. Parker†, Rodney L. Anderson‡, and George H. Born§

Autonomous orbit determination for departure stages of interplanetary trajectories is conducted by means of realistic radiometric observations between the departing spacecraft and a satellite orbiting the first lunar libration point. Linked Autonomous Interplanetary Satellite Orbit Navigation (LiAISON) is used to estimate the orbit solution. This paper uses high-fidelity simulations to explore the utilization of LiAISON in providing improved accuracy for interplanetary departure missions. The use of autonomous navigation to supplement current techniques for interplanetary spacecraft is assessed using comparisons with ground-based navigation. Results from simulations including the Mars Science Laboratory, Mars Exploration Rover, and Cassini are presented. It is shown that observations from a dedicated LiAISON navigation satellite could be used to supplement ground-based measurements and significantly improve tracking performance.

INTRODUCTION

Most observations used to navigate interplanetary spacecraft are carried out by means of Earth-based tracking sensors.¹ The large cost associated with Earth-based tracking and trajectory design has driven research into alternatives to ground operations as the primary means by which deep space missions are conducted.² Recent research has shown that the use of satellite-to-satellite tracking (SST) is one alternative that gives accurate absolute navigation.^{3,4} A new technique for performing this type of navigation is Linked Autonomous Interplanetary Satellite Orbit Navigation (LiAISON).⁵ LiAISON is conducted between two or more spacecraft accumulating relative radiometric tracking data to simultaneously estimate their relative and absolute positions and velocities over time.⁵

LiAISON is enabled by unique trajectories created by the asymmetry in the acceleration field governed by three-body dynamics. Halo orbits about the Earth Moon L_1 (EML-1) point exhibit these characteristics and are used for this study. Though SST measurements generally provide relative orbit determination between spacecraft even in unperturbed acceleration fields, under the influence of the acceleration of the Moon the halo satellite is effectively tied to the Earth-Moon system and can therefore provide absolute position and velocity estimation for a variety of other orbits. Thus, the advantage of this architecture comes from the fact that while a constellation of satellites orbiting under dynamics without significantly detectable perturbations will provide only relative trajectory information on any satellite included, LiAISON provides precise knowledge of the absolute states of each spacecraft. While LiAISON has been shown to improve accuracy for satellite navigation in the Earth-Moon vicinity, it has yet to be applied to Interplanetary departure trajectories. In this study we demonstrate the situational geometry present in the interplanetary departure problem, as geometrical improvements to conventional ground-based orbit determination (OD) techniques are the source of advantage for the LiAISON architecture.

*Graduate Research Assistant, University of Colorado, Boulder, CO 80309

†Research Professor, Colorado Center for Astrodynamics Research, University of Colorado, Boulder, CO 80309

‡Member of Technical Staff, Jet Propulsion Laboratory, California Institute of Technology, M/S 301-121, 4800 Oak Grove Dr., Pasadena, CA 91109

§Director Emeritus, Colorado Center for Astrodynamics Research, University of Colorado, Boulder, CO 80309

The performance and advantage of LiAISON has been demonstrated in several papers, including in support of precise orbit determination of geosynchronous spacecraft,^{6,7,8} and in providing navigation solutions for lunar-bound missions, including low-lunar orbiters and lunar libration orbiters.^{1,3,5} In fact, a concurrent study is characterizing the performance of LiAISON-supported navigation for very noisy crewed missions bound for the Moon.^{9,10}

The only operational EM-LPO navigation experience currently available was obtained through the ARTEMIS mission which traversed both EML-1 and EML-2 trajectories.¹¹ The two ARTEMIS spacecraft arrived in the lunar libration regime in late 2010 and departed to low lunar orbits in mid 2011. Extensive ground support from the Deep Space Network (DSN), Universal Space Network (USN), and Berkeley Ground Station (BGS) provided radiometric tracking measurements.^{12,13} The nominal strategy during this period was to collect 3.5 hours of DSN range and Doppler information each day, alternating between northern and southern hemispheres, and supplementing this with daily tracks from BGS and a weekly track of USN.¹² The tracking design produced accuracies for each satellite of 100 meters in position and down to 1 mm/s in velocity.¹²

This paper discusses in depth a new paradigm in orbit determination, LiAISON, and the benefits observed in utilizing it in the departure phase of interplanetary trajectories. The simulations we develop and discuss use relative satellite-to-satellite observations between a dedicated navigation satellite in an EML-1 lunar libration point orbit (LPO) and a spacecraft departing on an interplanetary trajectory to determine the absolute positions and velocities of both satellites. The focus is to provide a quantitative analysis in ground station-supplemented orbit determination solutions as well as standalone solutions using LiAISON in a high-fidelity simulation. We show that LiAISON provides improved navigation accuracy for interplanetary trajectories when used to supplement ground-based observations.

The study begins by detailing the performance of the DSN using continuous tracking of the outbound trajectories under specified simulation conditions. Next, the DSN solutions are quantitatively compared with the navigation solution tracking the same trajectory using only LiAISON observations. Finally, DSN and LiAISON observations are taken simultaneously in the realistic situation where SST would be used to supplement ground station tracking. In each case realistic radio measurements serve as the observables in the solution process. Additionally, the simulations include dynamical modeling errors, measurement errors, and measurement biases. The interplanetary trajectories used in this analysis were the Cassini, Mars Exploration Rover A (MER A), and Mars Science Laboratory (MSL) spacecraft.

LIAISON NAVIGATION

LiAISON is the performance of absolute tracking of two or more spacecraft using relative SST measurements without the aid of groundstation observations. The determination of orbit size, shape, and orientation are each necessary to provide absolute tracking. The key is that the SST measurement time-series can only be generated using a unique combination of orbits. A trajectory is unique when only a single set of initial conditions exist that result in an orbit of that size and shape. The acceleration field governing a satellite's orbit determines whether a unique trajectory can exist, and this is only possible where the acceleration function and its time derivative are appreciably asymmetric. Therefore, LiAISON navigation relies on one of the linked spacecraft being under the influence of asymmetric dynamics. In fact, the asymmetry must be sufficient enough to outweigh force modeling errors and observation noise to prevent being lost beneath the noise during the orbit determination process.

Three-body systems provide sufficient asymmetry to create observability in the LiAISON process. Specifically, perturbations provided by the Moon give rise to LPOs whereby LiAISON is well-suited. The libration point residing between the Earth and Moon, EML-1, gives rise to locally unique trajectories with significant asymmetry in the governing acceleration function. This asymmetry allows absolute positioning to be performed by means of SST alone. Though orbits about EML-1 were used for this study, spacecraft placed about EML-2 would work just as well. In fact, these may be even better suited for tracking interplanetary missions due to their distance from Earth.

LiAISON has been demonstrated for several navigation applications using LPOs.^{3,5,14} Early research analyzed the benefits of this system using EML-1 and EML-2 orbits to track low lunar orbits and several

permutations therein.^{3,5} The results show that navigation solutions at the Moon with accuracies under 100 meters for the halo orbiters and an order of magnitude less for low lunar orbiting spacecraft are possible with realistic constraints and without the aid of ground tracking. More recently, studies have detailed precise orbit determination solutions for geosynchronous spacecraft using LiAISON navigation.^{6,7,8} Leonard et al. explored a trade study for geosynchronous spacecraft navigation with tracking from ground stations and a dedicated LiAISON satellite at EML-1.⁷ High-fidelity simulations produced viable tracking schedules that drastically reduced the ground station passes necessary for a given GEO position accuracy when LiAISON was included. Accuracies of 100 meters and 30 meters for the EML-1 and GEO satellites, respectively, were achieved using only sparse observations from the ground and LiAISON.

The application explored in this paper focuses LiAISON capabilities on the departure stage of interplanetary trajectories. We investigate the effectiveness of LiAISON in the departure phase of interplanetary missions by placing a dedicated navigation satellite at an EML-1 LPO and simulating the performance for three landmark NASA missions. Analysis is included for the Cassini, MER A, and MSL missions. Tracking expensive interplanetary missions in the departure phase is crucial to mission success through early trajectory correction maneuver design as well as pre-flight dynamical model calibration. Therefore, OD solutions for ground-tracking-only, LiAISON-only, and DSN supplemented with LiAISON navigation are analyzed to assess the potential value of using LiAISON in this context. Radiometric data with realistic errors and uncertainties comprise the observational model. The satellite orbits are determined using high-fidelity dynamical models and a Kalman filter is used to process the observations.

DYNAMICAL MODEL AND LINEARIZATION

The OD procedure begins with an initial estimate of a satellite state at a given epoch whose state and uncertainty are propagated through time yielding the reference trajectory. This path will deviate from that actually followed by the spacecraft, the truth trajectory. The OD procedure processes observations of the spacecraft to determine a new estimate of the reference path, the best estimate trajectory, that matches the true trajectory as well as possible. Thus, a linearization about the reference orbit is carried out and the process solves for state deviation vectors used to improve the reference. This section details the dynamical system governing the time evolution of the reference trajectory and the linearization process used in this study.

Dynamical Model

The propagation of the reference trajectory is governed by an approximation to the dynamics driving the truth trajectory. This approximation is given by a nonlinear first-order system of differential equations specified for this work as

$$\begin{bmatrix} \dot{\mathbf{r}}_i \\ \dot{\mathbf{v}}_i \end{bmatrix} = \begin{bmatrix} \mathbf{v}_i \\ \mathbf{a}_{2-body}(t, \mathbf{r}_i) + \mathbf{a}_{n-body}(t, \mathbf{r}_i) + \mathbf{a}_{SRP}(t, \mathbf{r}_i) \end{bmatrix} \quad (1)$$

where \mathbf{a}_{2-body} represents the acceleration due to Earth's gravitational pull, \mathbf{a}_{n-body} accounts for the gravitational accelerations of bodies outside the spacecraft-Earth system, and \mathbf{a}_{SRP} accounts for the effect of solar radiation pressure.

The two-body acceleration term is given as

$$\mathbf{a}_{2-body} = -\mu \begin{bmatrix} \mathbf{r}_{sat} \\ r_{sat}^3 \end{bmatrix} \quad (2)$$

where μ is the gravitational parameter of the primary body and \mathbf{r}_{sat} is the vector from the primary to the satellite.

The acceleration due to non-central bodies (n-bodies) are encapsulated in the \mathbf{a}_{n-body} term given as

$$\mathbf{a}_{n\text{-body},k} = -\mu_k \left[\frac{\mathbf{r}_{k,sat}}{r_{k,sat}^3} + \frac{\mathbf{r}_{\oplus,k}}{r_{\oplus,k}^3} \right] \quad (3)$$

where μ_k is the gravitational parameter of the k^{th} body, $\mathbf{r}_{k,sat}$ is the vector from the k^{th} body to the satellite, and $\mathbf{r}_{\oplus,k}$ is the vector from the central-body to the k^{th} body. These bodies introduce perturbations due to the Sun, Moon, or other heavenly bodies in the solar system. The Jet Propulsion Laboratory's DE405 ephemeris is used to compute the positions of the celestial bodies.^{15,16} Additionally, due to the great distances between the satellites and the bodies exerting gravitational influences, simplified point mass representations are used for all bodies.

Finally, a solar radiation pressure model is included in the force model for the satellite. This acceleration is based off of a constant area constant reflectance model. A shadow model calculates the portion of the Sun's surface visible to the satellite using radii of solar system bodies provided by the JPL ephemerides.¹⁵ The acceleration is additionally adjusted for distance from the Sun. This acceleration becomes

$$\mathbf{a}_{SRP} = P_{SR} C_R \frac{A_{\odot}}{m} \frac{\mathbf{r}_{\odot sat}}{r_{\odot sat}} \quad (4)$$

where C_R is the coefficient of reflectivity for the spacecraft, A_{\odot} is the cross-sectional area of the spacecraft facing the Sun in square meters, m is the mass of the spacecraft in kilograms, $\mathbf{r}_{\odot sat}$ is the vector from the center of the Sun to the spacecraft, and P_{SR} is the pressure of the solar radiation in pascals. P_{SR} is about 4.53×10^{-6} Pa at one AU and can be calculated at varying distances from the Sun using

$$P_{SR} = P_{SR,AU} \frac{(149,597,870 \text{ km})^2}{r_{\odot sat}^2} \quad (5)$$

The dynamical system governing the evolution of the state, \mathbf{X} , can be assembled and written as

$$\dot{\mathbf{X}}(t) = \mathbf{f}(t, \mathbf{X}(t), \mathbf{u}(t)) \quad (6)$$

where $\mathbf{u}(t)$ is a zero-mean Gaussian white process noise vector. This represents a first order ordinary differential equation that can be solved using integration.

Linearization of the Dynamical Model

The orbit determination procedure seeks to estimate a set of selected variables, in this case the position and velocity of the interplanetary (ip) and EML-1 halo (h) satellites. Therefore, the state becomes

$$\mathbf{X} = [x_{ip}, y_{ip}, z_{ip}, \dot{x}_{ip}, \dot{y}_{ip}, \dot{z}_{ip}, x_h, y_h, z_h, \dot{x}_h, \dot{y}_h, \dot{z}_h] \quad (7)$$

In order to perform the estimation, the state dynamics are linearized about a reference trajectory, \mathbf{X}^* , which in this study is taken to be the current best estimate trajectory. We can now define our state deviation vector to be

$$\mathbf{x}(t) = \mathbf{X}(t) - \mathbf{X}^*(t) \quad (8)$$

with $\mathbf{X}(t)$ representing the unknown truth trajectory. The state deviation vector can be mapped from one epoch to another using the state transition matrix

$$\Phi(t_{k+1}, t_k) = \frac{\partial \mathbf{X}(t_{k+1})}{\partial \mathbf{X}(t_k)} \quad (9)$$

and the process noise transition matrix

$$\mathbf{\Gamma}(t_{k+1}, t_k) = \frac{\partial \mathbf{X}(t_{k+1})}{\partial \mathbf{u}(t_k)} \quad (10)$$

The state transition matrix can be found for any time the reference trajectory has been integrated by solving the system of differential equations

$$\dot{\mathbf{\Phi}}(t, t_k) = A(t)\mathbf{\Phi}(t, t_k) \quad (11)$$

with initial conditions $\mathbf{\Phi}(t_0, t_0) = I$. The matrix $A(t)$ is given by the Jacobian matrix

$$A(t) = \frac{\partial f(t, \mathbf{X}(t))}{\partial \mathbf{X}(t)} \quad (12)$$

Finally, the state transition matrix is used to map the state deviation through time

$$\mathbf{x}(t_{k+1}) = \mathbf{\Phi}(t_{k+1}, t_k)\mathbf{x}(t_k) + \mathbf{\Gamma}(t_{k+1}, t_k)\mathbf{u}(t_k) \quad (13)$$

OBSERVATIONAL MODEL AND LINEARIZATION

In order to determine the state of the spacecraft at some future epoch, it must be observed from tracking stations, which could be ground stations or, in the case of LiAISON, a dedicated navigation satellite. These observations are processed in the OD filter to drive the state and uncertainty updates. The filtering process seeks the initial state of the satellite that minimizes the computed residual, observed minus expected, based off of the current best estimate trajectory, for some defined cost function. Much like the dynamical model, the filter requires a measurement model and its linearized representation; this section details that process.

Measurement Model

This study implements a simplified measurement model. Simulated observed instantaneous range and range-rate measurements are generated using each state along the truth trajectories for the halo and interplanetary departing spacecraft. More realistic measurements including time of flight and clock effects are not included in this proof of concept paper, but must be for future realistic mission analyses. The observed measurement model then becomes

$$\mathbf{Y}_o(t) = \mathbf{h}(t, \mathbf{X}(t)) = \begin{bmatrix} \rho(t) + \rho_{noise} + \rho_{bias} \\ \dot{\rho}(t) + \dot{\rho}_{noise} \end{bmatrix} \quad (14)$$

Idealized equations for ρ and $\dot{\rho}$ are used in this study. These are given in Eqs. 15 and 16.

$$\rho = \sqrt{(x_h - x_{ip})^2 + (y_h - y_{ip})^2 + (z_h - z_{ip})^2} + \rho_{noise} + \rho_{bias} \quad (15)$$

$$\dot{\rho} = \frac{\boldsymbol{\rho} \cdot \dot{\boldsymbol{\rho}}}{\rho} + \dot{\rho}_{noise} \quad (16)$$

The range measurements are corrupted by adding constant bias and Gaussian white noise terms. The range-rate corruption is contained in the white noise addition shown in Eq. 16.

Similarly, simulated ground station observations are found with these equations, where one of the states is replaced by the coordinates of the given observing station in GCRF coordinates. For the purposes of this work, ground station locations were chosen from the three main DSN sites; Goldstone, Madrid, and Canberra.

The measurement model is also used to generate expected observations. The satellite states along the reference trajectories are used in place of the truth trajectories. The residuals are found when the expected and observed measurements are differenced

$$\epsilon = \mathbf{Y}_o - \mathbf{Y}_e \quad (17)$$

The filtering process will minimize the residuals due to criteria specified in some cost function.

Linearization of the Measurement Model

In a similar manner to how we derived the state deviation mapping equation, we also seek an equation by which the observations can be mapped through time. To do so, the observation deviation vector, \mathbf{y} , at the current epoch must be given in terms of the state deviation vector at the reference epoch, t_0

$$\mathbf{y}(t_k) = H(t_k)\mathbf{x}(t_0) + \epsilon(t_k) \quad (18)$$

where the state transition matrix is again used to perform the mapping

$$\mathbf{y}(t_k) = H(t_k)\Phi(t_0, t_k)\mathbf{x}(t_0) + \epsilon(t_k) \quad (19)$$

This is simplified to

$$\mathbf{y}(t_k) = \tilde{H}(t_k)\mathbf{x}(t_0) + \epsilon(t_k) \quad (20)$$

with the relationship $\tilde{H}(t_k)\Phi(t_0, t_k) = H(t_k)$. Finally, the linearization process produces the Jacobian matrix to construct the $\tilde{H}(t)$ matrix as follows

$$\tilde{H}(t) = \frac{\partial \mathbf{h}(t, \mathbf{X}(t))}{\partial \mathbf{X}(t)} \quad (21)$$

ORBIT DETERMINATION FILTER

In this study an attempt is made at estimating the state given in Eq. 7 using a Kalman filter. The Kalman update equations begin with *a priori* estimates of both the state deviation vector, $\hat{\mathbf{x}}(t_k)$, and associated covariance matrix, $\bar{P}(t_k)$ and propagate them forward in time using the time update equations

$$\bar{\mathbf{x}}(t_{k+1}) = \Phi(t_{k+1}, t_k)\hat{\mathbf{x}}(t_k) \quad (22)$$

$$\bar{P}(t_{k+1}) = \Phi(t_{k+1}, t_k)P(t_k)\Phi(t_{k+1}, t_k)^T + \Gamma(t_{k+1}, t_k)Q(t_k)\Gamma(t_{k+1}, t_k)^T \quad (23)$$

Where the second term in Eq. 23 represents the state noise compensation (SNC) contribution to the *a priori* covariance term called the process noise covariance matrix. $Q(t_k)$ is given by

$$E[\mathbf{u}(t)\mathbf{u}^T(\tau)] = Q(t_k)\delta(t - \tau) \quad (24)$$

where δ is the Dirac Delta.

In the presence of errors in the dynamical model, as the number of accurate observations increases, the covariance matrix will asymptotically approach zero making the estimation procedure insensitive to new observations and force the results to diverge. SNC is used to account for dynamical model errors and prevent

this divergence. In this study, the process noise covariance matrix will be diagonal and chosen by a trial and error approach to best represent un-modeled accelerations.

Assuming an observation exists at t_{k+1} , the next epoch in the simulation, the linearized equation can be written

$$\mathbf{y}(t_{k+1}) = \tilde{H}(t_{k+1})\mathbf{x}(t_{k+1}) + \boldsymbol{\epsilon}(t_{k+1}) \quad (25)$$

where \mathbf{y}_{k+1} signifies the deviations in the observations between the truth and the computed measured on the reference trajectory, $\boldsymbol{\epsilon}_{k+1}$ represents measurement noise and errors, and $\tilde{H}(t_{k+1})$ was defined in Eq. 21. Subsequently, the best state estimate is given through the measurement update equations

$$\hat{\mathbf{x}}(t_{k+1}) = \bar{\mathbf{x}}(t_{k+1}) + K(t_{k+1})[\mathbf{y}(t_{k+1}) - \tilde{H}(t_{k+1})\bar{\mathbf{x}}(t_{k+1})] \quad (26)$$

$$K(t_{k+1}) = \bar{P}(t_{k+1})\tilde{H}(t_{k+1})^T[\tilde{H}(t_{k+1})\bar{P}(t_{k+1})\tilde{H}(t_{k+1})^T + R(t_{k+1})]^{-1} \quad (27)$$

$$P(t_{k+1}) = [I - K(t_{k+1})\tilde{H}(t_{k+1})]\bar{P}(t_{k+1}) \quad (28)$$

Where $K(t_{k+1})$ represents the Kalman Gain and $R(t_{k+1})$ is the measurement error covariance matrix. The covariance update equation, given by Eq. 28, can exhibit numerical problems throughout the filtering process, so for this study a more stable update equation given by the Joseph Formulation is used and given by

$$P(t_{k+1}) = [I - K(t_{k+1})\tilde{H}(t_{k+1})]\bar{P}(t_{k+1})[I - K(t_{k+1})\tilde{H}(t_{k+1})]^T + K(t_{k+1})R(t_{k+1})K(t_{k+1})^T \quad (29)$$

The equations for the development of the dynamic, observation, and filter models were guided by the discussion given by Born, et al. in Ref. 17.

TRUTH MODEL SIMULATIONS

To assess the performance of the filter, a truth model simulation can be used. The truth model is realized through numerical integration of the equations of motion given in the *Dynamical Model and Linearization* section of this paper. A DOPRI8(7)13 integrator with variable step size control was used to generate high-fidelity truth trajectories for this study.¹⁸ Radiometric tracking of the spacecraft is simulated between both the two orbiters, for LiAISON observations, and from the DSN stations. The orbit integration package, TurboProp, is used to solve the time evolution of the state dynamics.¹⁹

EML-1 Truth Model

The EML-1 truth trajectory is integrated in the GCRF coordinate frame using third body perturbations of all solar system planets including the Moon. The state of each body is provided by the JPL DE405 ephemeris.¹⁵ Each body is modeled as a point mass. Additionally, the simple solar radiation pressure approximation given in Eq. 4 is used with an area-to-mass ratio and C_R of 0.01 m²/kg and 1.5, respectively.

The L_1 reference trajectory is generated in two steps. First, a set of states is obtained from the analytical expansion described in Ref. 20 using the dates given in Table 1 for the appropriate simulation. A single shooting process is then used to differentially correct these states into the high-fidelity dynamical model discussed previously.^{21,22} The purpose of the differential corrector is to create a continuous trajectory such that the orbit between the states contains no discontinuities greater than 10^{-6} km in position and 10^{-9} km/s in velocity. Normal operational navigation of halo orbiters contain uncertainties greater than these constraints, and therefore this is considered appropriate for the designation of a continuous trajectory.

Interplanetary Spacecraft Truth Models

The interplanetary departure trajectory truth models are generated in a manner similar to the process detailed for the EML-1 spacecraft. The same dynamical system is used. Again, the Earth and all gravitational forces are modeled as point masses. This is valid despite the interplanetary satellites beginning near Earth due to the fact that each rapidly moves away from the region where spherical harmonics representations at Earth are considered valid and point mass representations become acceptable.¹⁷ The single shooting differential corrector is used in this case to specify the trajectory between the initial and final epochs of the overall measurement arc chosen for the departure stage of each mission. Table 1 contains the initial and final epochs used in the simulations.

Measurement Generation

LiAISON measurements are taken between the halo and interplanetary departure spacecraft throughout the simulation period. Both instantaneous range and range-rate are used for the SST measurements as given by Eq. 15 and Eq. 16. The LiAISON observations are corrupted by Gaussian white noise with zero mean and $1-\sigma$ standard deviations of 1 m and 1mm/s, respectively. Simulated DSN ground stations are used to generate Earth-based observations. Zero mean Gaussian white noise is introduced to corrupt these measurements as well, with 1 m and 0.1 mm/s $1-\sigma$ standard deviations. A bias taken from a uniform distribution with 3 m $1-\sigma$ standard deviation is additionally included in the range measurement corruption for both sets of observations. Only one DSN observation is included per epoch in this study, even in situations where the satellites are visible by more than one ground station. To select these measurements, highest weight is placed on the Goldstone station, followed by Madrid, and finally Canberra. The *a priori* uncertainties for the measurement model are given in Table 2.²³ Lastly, all observations are taken and processed sequentially in the Kalman filter at 1000 second intervals throughout the 9 day measurement arc.

NAVIGATION RESULTS

This section begins by detailing the baseline orbit determination filter set-up including the dynamical model used, initial state errors, and *a priori* uncertainties. It goes on to display and discuss the results and filter performance for the Cassini, MER A, and MSL mission departure trajectories. Performance was analyzed for three observational situations: LiAISON-only, DSN-only, and DSN supplemented with LiAISON. Note that in the LiAISON-only simulation the EML-1 satellite is established as a dedicated navigation satellite and thus it is tracked by the ground. LiAISON-only refers to the fact that the interplanetary spacecraft is only observed by SST measurements.

Orbit Determination Filter Set-up

In order to assess filter performance in a real-world situation, dynamical modeling errors were introduced to the reference trajectory used in the filter. Third-body effects were again introduced, however instead of each planet in the solar system contributing to the force model, only the gravitational influences of the Earth central body, Moon, and Sun were modeled in the filter. SRP still perturbed the trajectories of each spacecraft, however the coefficient of reflectivity was initially randomly perturbed from a standard deviation of 5% of the C_R values. The DSN station positions were considered known and were not estimated. However, the state of the navigation satellite at EML-1 for all simulations was estimated along with the interplanetary departing spacecraft. SNC was implemented to compensate for the unmodeled accelerations. Note that the SNC levels used were tailored specifically for the full and LiAISON-only set-ups to give the best results in each.

Table 1: A summary of the interplanetary departure trajectory truth models.

Trajectory	Initial Epoch	Final Epoch
Cassini	Oct 15, 1997 9:35:42.8824	Oct 24, 1997 9:35:42.8824
Mars Exploration Rover A	Jun 10, 2003 18:31:23.1840	Jun 19, 2003 18:31:23.1840
Mars Science Laboratory	Nov 26, 2011 15:52:12.3830	Dec 5, 2011 15:52:12.3830

Table 2: A summary of the orbit determination filter uncertainties used throughout the simulations.

Estimation Parameter	<i>a priori</i> Uncertainty (1-sigma)	Number of Filtered Parameters
Spacecraft Position		
(EML-1 Satellite)	20 (m)	3
(Interplanetary Satellite)	1000 (m)	3
Spacecraft Velocity		
(EML-1 Satellite)	0.1 (mm/s)	3
(Interplanetary Satellite)	10 (m/s)	3
SRP Coefficient	5 %	-
SST Measurements		
Range	1 (m)	-
Range-rate	1 (mm/s)	-
DSN Measurements		
Range	10 (m)	-
Range-rate	0.5 (mm/s)	-
SST Range Bias (randomly drawn)	3 (m)	-
DSN Range Bias (randomly drawn)	3 (m)	-

Filter runs using the full set of observations (LiAISON and DSN) were used in addition to literature on each mission to determine the *a priori* uncertainties. Uncertainties that provided solutions as accurately as possible and subject to realistic operational values were chosen. The uncertainty in both position and velocity of the EML-1 spacecraft were reduced assuming that observations of this orbit prior to the interplanetary trajectory departure date would allow the state to be known more accurately. Previous LiAISON studies have demonstrated the ability to accurately determine the state of an EML-1 satellite and explain the chosen uncertainty levels given in Table 2.^{1,5,6,7,8} Measurement noise uncertainties were chosen to be consistent with modern operational orbit determination, specifically values used for the Gravity Recovery and Interior Laboratory Mission (GRAIL).²⁴ Extremely large initial state uncertainties were used for the GRAIL mission, however smaller values were deemed acceptable in this work. The values determined and detailed in Table 2 were used for each simulation throughout the study. Filter performance was assessed in each case to ensure consistency and reliability of results. Comparisons of the estimated states with truth models were conducted to ensure results were both reasonable and remained within uncertainty bounds and provided a metric for filter performance overall.

Finally, the technical aspects of each of these mission trajectories are well published in literature and will not be detailed in this paper for the sake of space. Instead the reader is referred to Refs. 25, 26, and 27 for technical information on Cassini, MER A, and MSL, respectively. States from the published, reconstructed trajectories have been used to model the truth trajectories in this study.

Cassini

The Cassini spacecraft departed Earth on 15 October, 1997 on a Venus-Venus-Earth-Jupiter-gravity assist (VVEJGA) trajectory. This section explores the filter’s ability to estimate the parameters in Eq. 7 for the first nine days of the mission. The simulation geometry is shown in Figure 1 in the Earth-Moon rotating frame.

Figs. 2 through 5 show the results from the Cassini simulations. The far left plots represent what will be referred to as the full set-up, processing range and range-rate observations from the DSN stations and LiAISON. The $3\text{-}\sigma$ covariance envelopes are provided as well. Due to the relatively limited motion of the Cassini spacecraft out of the XY plane, a lack of knowledge of the z-direction contributed to larger errors and uncertainties shown in Figs. 4 and 5. However, these figures show that despite the higher errors in the

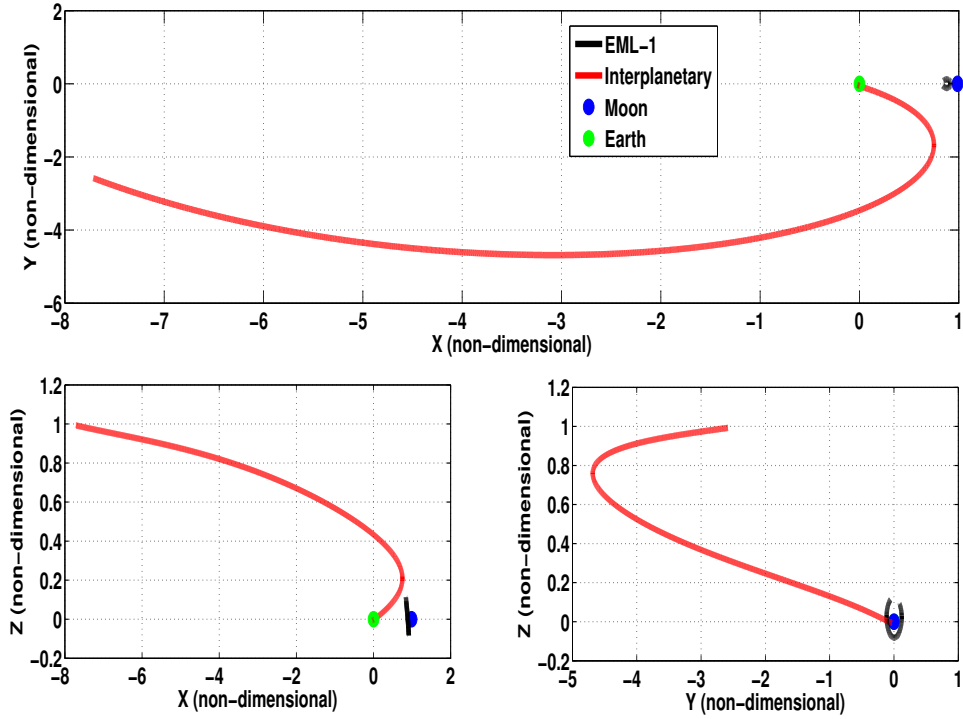


Figure 1: Views of the Cassini simulation geometry in the Earth-Moon rotating frame with nondimensional coordinates. The X-Y plane (top), X-Z plane (bottom left), and Y-Z frame (bottom right) are shown.

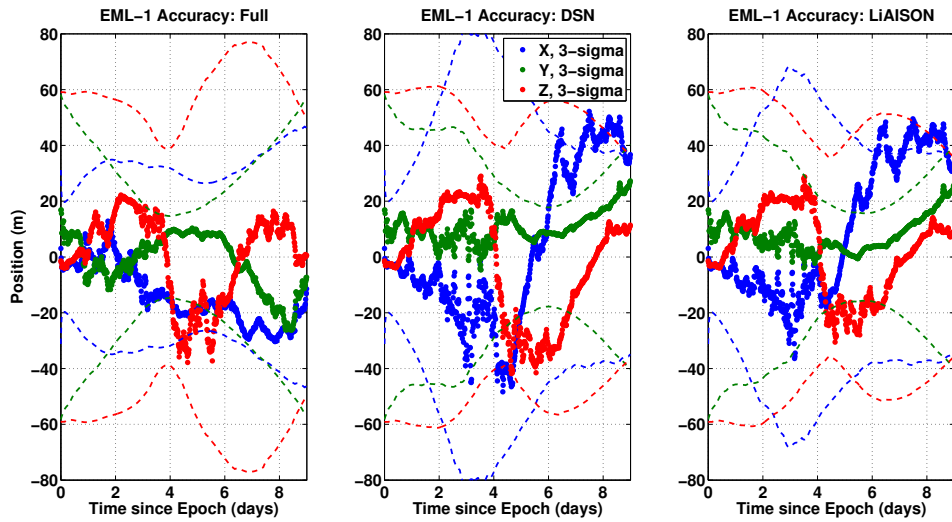


Figure 2: EML-1 satellite position accuracies (truth - estimated) and 3-sigma uncertainty envelopes for the full (left), DSN-only (middle), and LiAISON-only (right) Cassini mission simulations.

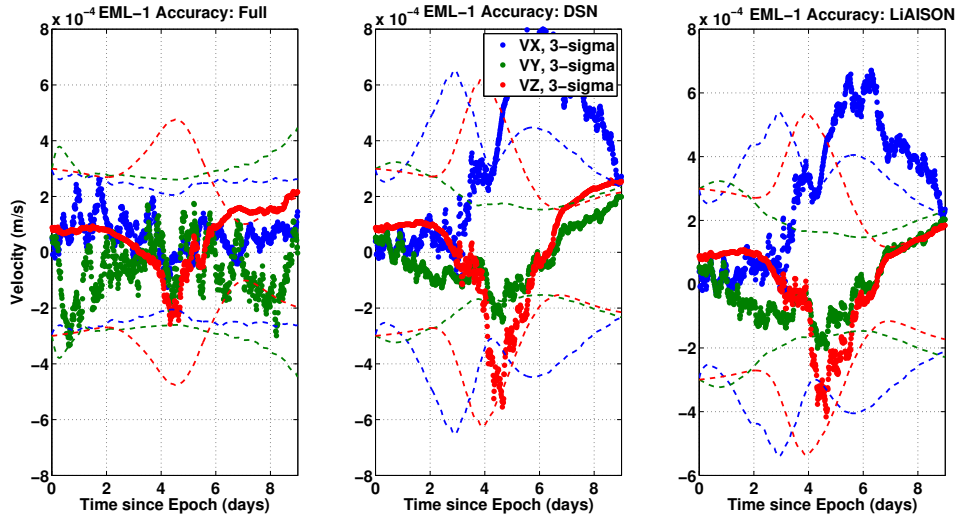


Figure 3: EML-1 satellite velocity accuracies (truth - estimated) and 3-sigma uncertainty envelopes for the full (left), DSN-only (middle), and LiAISON-only (right) Cassini mission simulations.

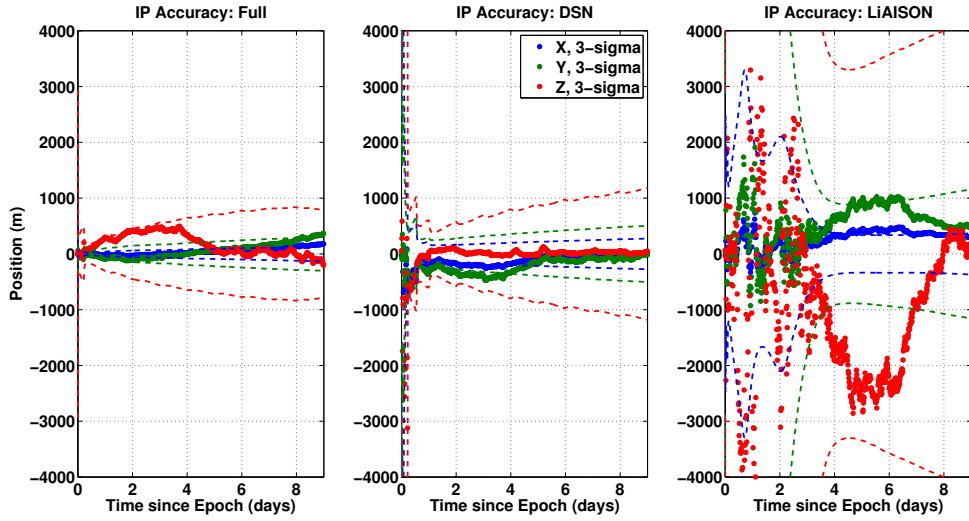


Figure 4: Interplanetary satellite position accuracies (truth - estimated) and 3-sigma uncertainty envelopes for the full (left), DSN-only (middle), and LiAISON-only (right) Cassini mission simulations.

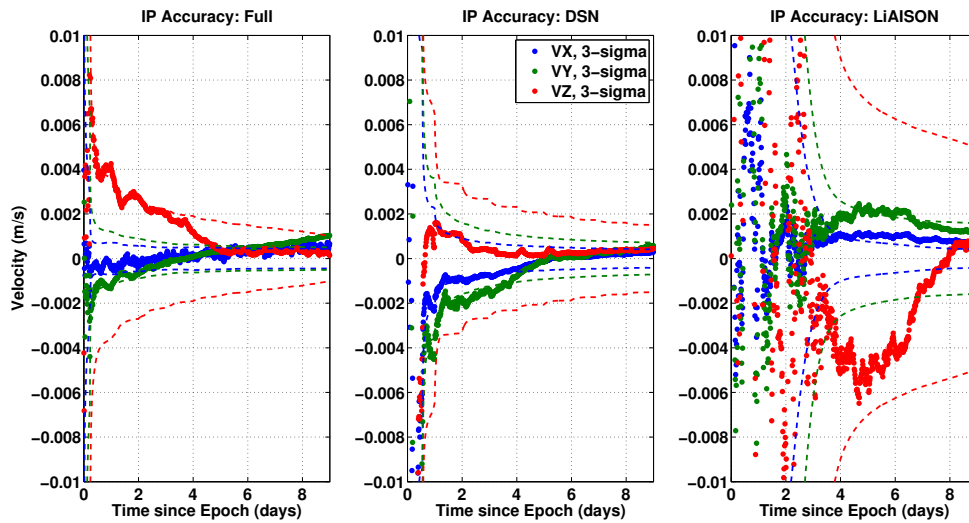


Figure 5: Interplanetary satellite velocity accuracies (truth - estimated) and 3-sigma uncertainty envelopes for the full (left), DSN-only (middle), and LiAISON-only (right) Cassini mission simulations.

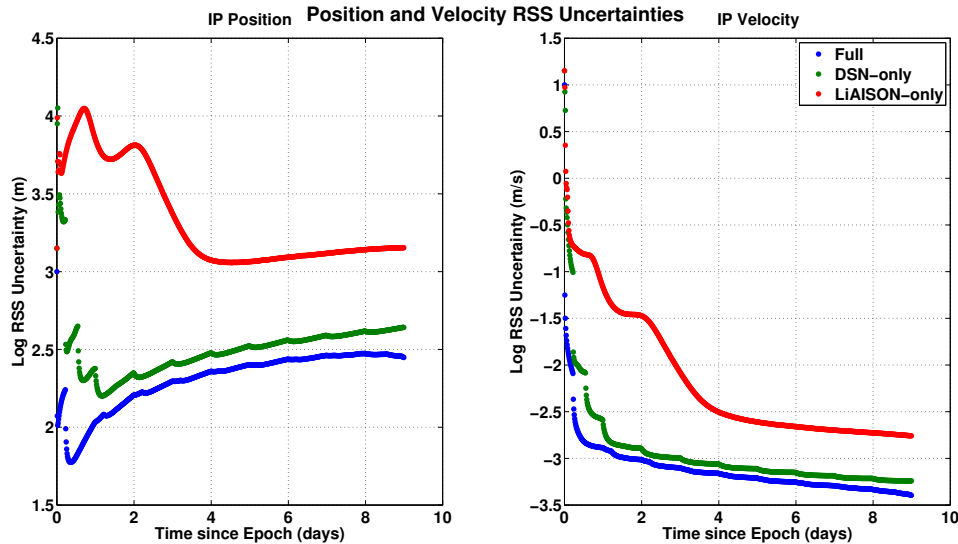


Figure 6: Log RSS uncertainties for the Cassini mission simulations. Uncertainties in the position (left) and velocity (right) are given for the EML-1 (top) and interplanetary (bottom) satellites.

LiAISON-only simulations, including observations from a dedicated navigation satellite at EML-1 tracked by the ground, the tracking performance of the DSN-only case was significantly improved when supplemented by the SST measurements. Using both measurements tightened the 3D-root mean square (RMS) uncertainty of the interplanetary spacecraft position by nearly 500 m and improved the 3D-RMS velocity uncertainty by a factor of two. Figure 6 gives the time evolution of the log root sum square (RSS) position and velocity uncertainties for each satellite. The DSN-only uncertainties (shown in green) were improved in both position and velocity for each satellite when used in concert with LiAISON observations (given by the full simulation values shown in blue).

Over the nine day simulation period the distances grew substantially and worsening 3-dimensional relative motion between Cassini and the Earth and between Cassini and the EML-1 satellite contributed to less effective observations. During this time, it appears that LiAISON navigation became even more important. Figure 4 shows that with DSN tracking alone the interplanetary position uncertainties continued to grow, however in the full simulation the uncertainties leveled off due to LiAISON navigation.

Filter results demonstrate that the EML-1 position and velocity uncertainties were maintained roughly at the *a priori* levels specified in the simulation and were relatively well known throughout. This is desired behavior for a navigation satellite. The 3D-RMS values for the EML-1 orbit uncertainties over the 9 day measurement arc in the full simulation were 26 m and 0.16 mm/s in position and velocity, respectively. The 3D-RMS values for the simulated Cassini spacecraft were 232 m and 0.36 m/s.

Mars Exploration Rover A

The Mars Exploration Rover project launched two rovers to the red planet in the summer of 2003. The focus of this section is the departure phase of the MER A spacecraft, which left Earth on 10 June, 2003. The geometry for this departure trajectory is shown in Figure 7 in the Earth-Moon rotating frame.

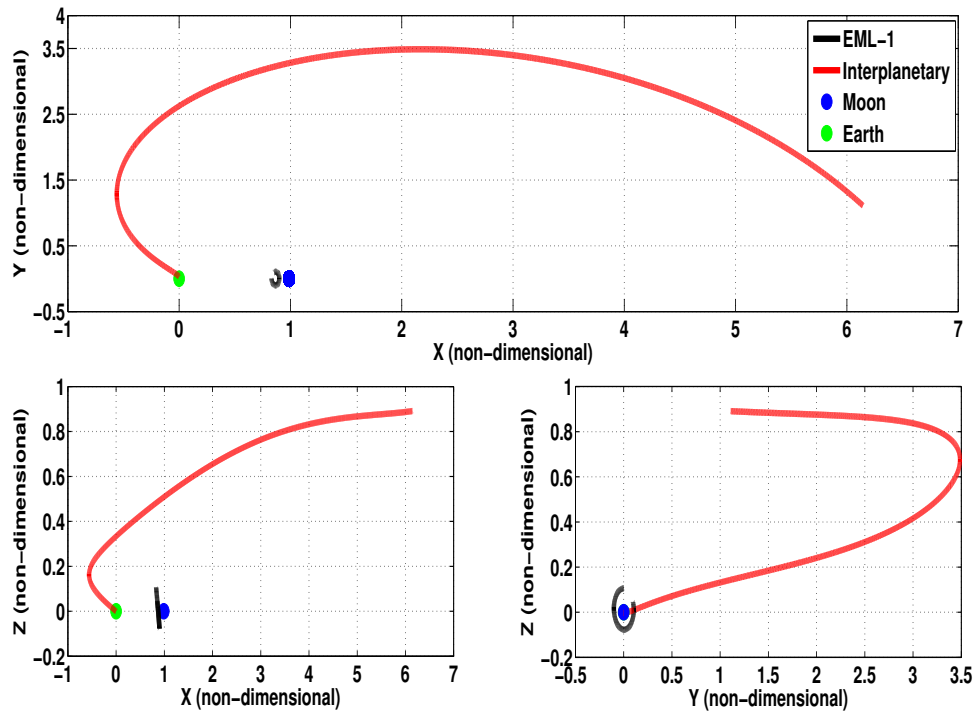


Figure 7: Views of the MER A simulation geometry in the Earth-Moon rotating frame with nondimensional coordinates. The X-Y plane (top), X-Z plane (bottom left), and Y-Z frame (bottom right) are shown.

The time history of the navigation performance for the MER A simulation is shown in Figs. 8 through 9. The LiAISON-only case shown in the right panel of Figure 8 gave better results than were found for the Cassini mission. Whereas the Cassini trajectory followed a path initially approaching the EML-1 orbit, it quickly moved away from the Moon creating problems for the LiAISON process. However, MER A traveled towards the Moon with respect to the Earth. Decreased uncertainties and errors for MER A due to SST show that geometry is an important factor in the performance of LiAISON. The behavior of the RSS uncertainty values shown in Figure 9 is comparable to Figure 6 and displays similar benefit in using LiAISON and DSN observations together. In the full simulation, MER A 3D-RMS uncertainty values were 194 m in position and 0.63 m/s in velocity.

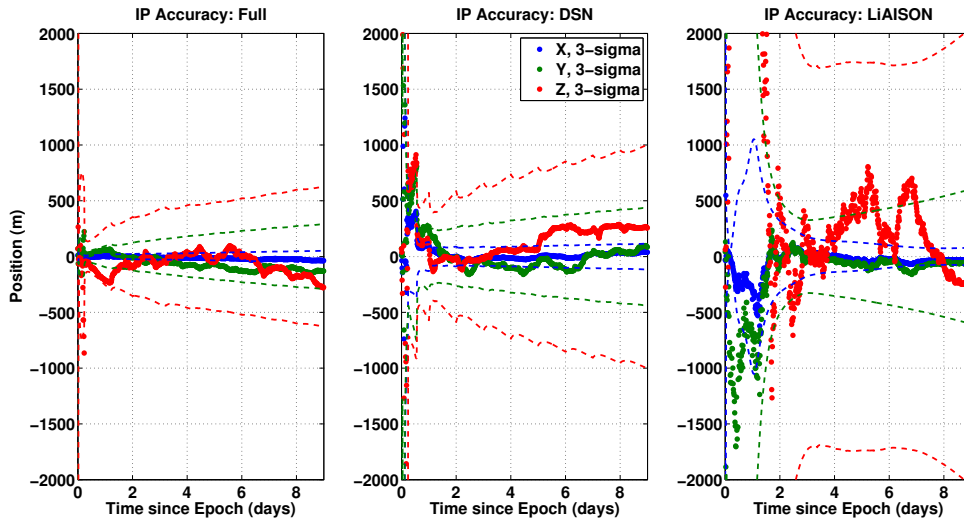


Figure 8: Interplanetary satellite position accuracies (truth - estimated) and 3-sigma uncertainty envelopes for the full (left), DSN-only (middle), and LiAISON-only (right) MER A mission simulations.

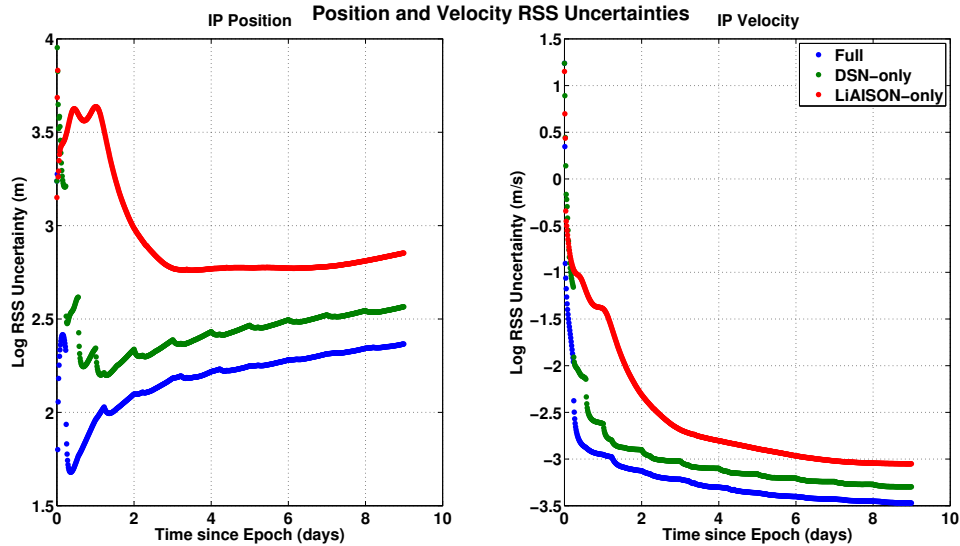


Figure 9: Log RSS uncertainties for the MER A mission simulations. Uncertainties in the position (left) and velocity (right) are given for the EML-1 (top) and interplanetary (bottom) satellites.

Mars Science Laboratory

This section is centered around assessing the filter performance using the MSL trajectory as the interplanetary departure orbit. MSL departed Earth on 26 November, 2011. Figure 10 is provided for the MSL mission geometry in the Earth-Moon rotating frame. Exploring the MSL trajectory presented a chance to analyze LiAISON performance for a different geometry so that the influence on navigation capability could be observed.

The MSL trajectory presented the most difficult geometry for LiAISON navigation. Figure 10 shows the trajectory moving away from the EML-1 orbit. Relatively large uncertainties accompanied this trajectory

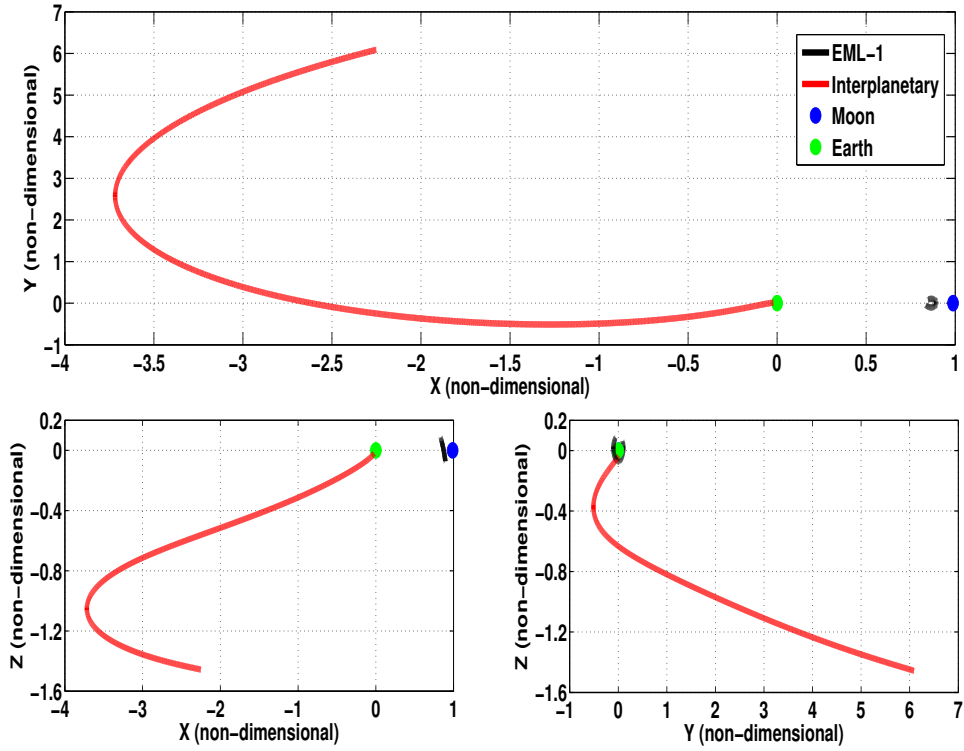


Figure 10: Views of the MSL simulation geometry in the Earth-Moon rotating frame with nondimensional coordinates. The X-Y plane (top), X-Z plane (bottom left), and Y-Z frame (bottom right) are shown.

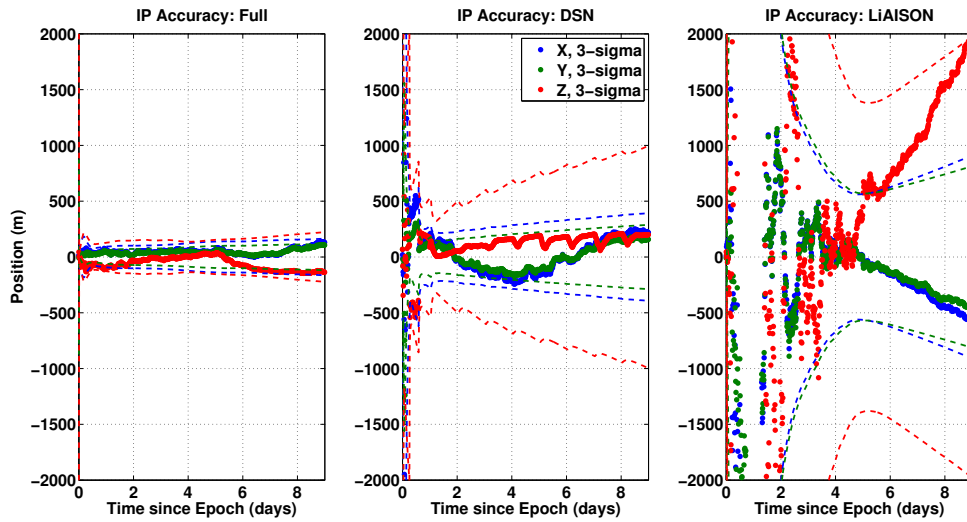


Figure 11: Interplanetary satellite position accuracies (truth - estimated) and 3-sigma uncertainty envelopes for the full (left), DSN-only (middle), and LiAISON-only (right) MSL mission simulations.

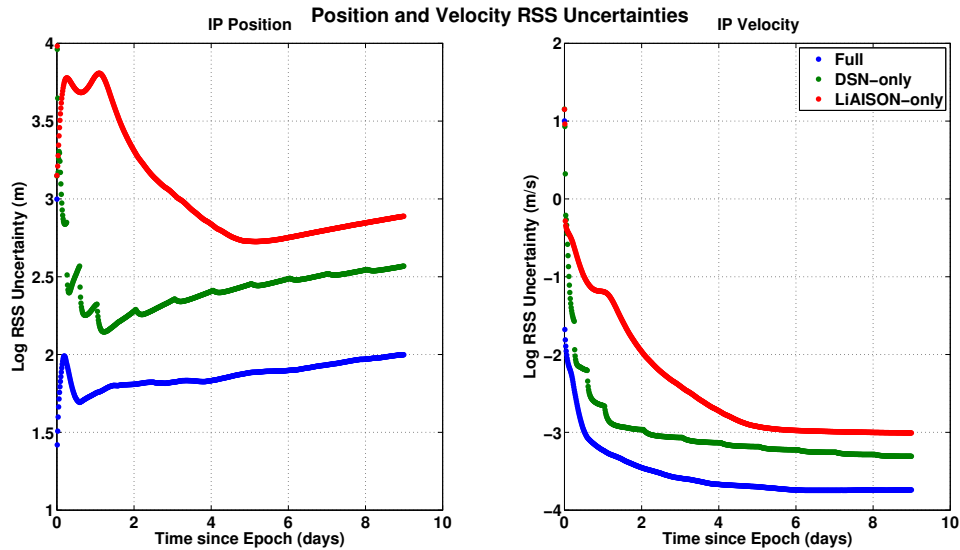


Figure 12: Log RSS uncertainties for the MSL mission simulations. Uncertainties in the position (left) and velocity (right) are given for the EML-1 (top) and interplanetary (bottom) satellites.

when only LiAISON was utilized. However, MSL exhibited the largest motion out of the XY-plane of the three missions studied in this report. As a result, the position uncertainties in the Z-direction (shown in Figure 11) were smaller for each simulation than those in Figs. 4 and 8 for Cassini and MER A, respectively. 84 m and 0.36 m/s 3D-RMS position uncertainty values in the full simulation were calculated for the simulated MSL spacecraft.

Mission Comparison

Table 3 contains the 3D-RMS values for each mission under the various simulations that were tested. These were calculated by taking the RSS of the x, y, and z coordinate errors and then calculating the RMS of these values. Only data from the second half of the measurement arcs (i.e. from day 4.5 and on) were used in these calculations to give a better representation of the filter performance once the initial uncertainties had been reduced. The table shows that LiAISON improved position accuracy significantly for the MER A and MSL missions. For Cassini, the higher 3D-RMS value for the full simulation can be attributed to the errors in LiAISON observations arising from poor geometry between days 3 and 6 of the simulation shown in Figure 14 and discussed below. Figure 4 shows a large error during this period in the position determination of the interplanetary spacecraft.

Figure 13 shows the RSS position errors compared for the three missions over each of the simulations. It is interesting to note that the LiAISON results show a clear spike in the position error for the Cassini spacecraft beginning near the 3.5 day mark and continuing for nearly 3 days. Figure 14 is provided to demonstrate the poor geometry that contributed to the heightened RSS error. During this period, the majority of the motion is directly away from the EML-1 satellite, increasing range primarily, with limited angular motion to allow LiAISON to gain 3D information.

LiAISON results showed that while it was less accurate than DSN when used alone, the benefit in supplementing ground station observations was significant both in position and velocity. The degradation in performance for LiAISON-only was most likely a result of two factors: 1) The assumption that these observations were less accurate than those from the ground and 2) the fact that the DSN stations were considered known and therefore not estimated. Though the state of the EML-1 navigation satellite was assumed relatively well known, the position and velocity were subject to initial perturbations and *a priori* uncertainties and were estimated in the filter. In the situation where the initial state was assumed known exactly, the *a priori*

Table 3: 3D position RMS values for the second half of each simulation.

Mission	Full Simulation (m)	DSN-Only (m)	LiAISON-Only (m)
Cassini (Interplanetary Satellite)	228.392	130.698	1874.312
MSL (Interplanetary Satellite)	133.890	254.462	1211.702
MER A (Interplanetary Satellite)	170.845	244.170	374.650

uncertainties were reduced, and SST observations were given the same accuracy as ground measurements, the LiAISON-only simulation exhibited uncertainties similar to the levels seen in DSN-only tracking.

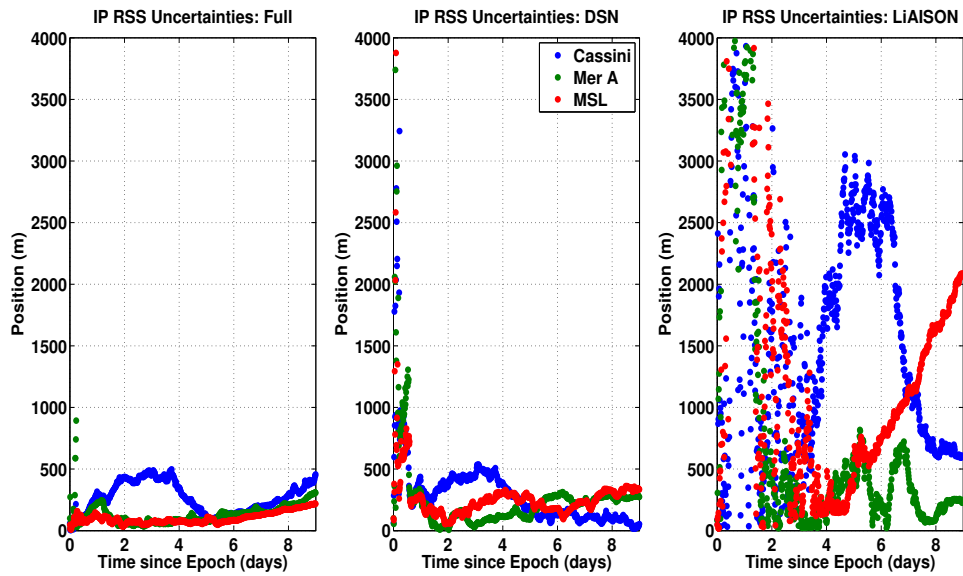


Figure 13: Interplanetary trajectories' RSS errors for each simulation.

EML-1-State-Fixed Simulations

We mention above that the LiAISON OD solutions must estimate both the state of the tracking station (the EML-1 navigation satellite) and the departing spacecraft. LiAISON is thus at a disadvantage with respect to ground-tracking simulations where the DSN locations were considered known. To investigate a more direct comparison between LiAISON and DSN performance, simulations for each mission were conducted where the EML-1 state was considered known and thus not estimated. Figure 15 shows the results for the MER A trajectory. The halo-state-known simulations used an extended Kalman filter (EKF) to process both range and range-rate observations. Dynamical errors and interplanetary spacecraft initial perturbations were included as before. However, the a priori uncertainty for the interplanetary spacecraft was 100 m and 0.1 m/s in position and velocity, respectively. Finally, observations were turned off for the first half day in these simulations. This allowed the dynamics to sufficiently affect the spacecraft state and more accurately gauge the filter's ability to recover the trajectory.

The benefit of the LiAISON system is clearly shown in Figure 15. Though the DSN is able to more quickly reduce the uncertainty, LiAISON outperforms ground-only tracking after roughly 4 days of observations. Additionally, where the DSN is unable to attain a steady state solution in these simulations, LiAISON

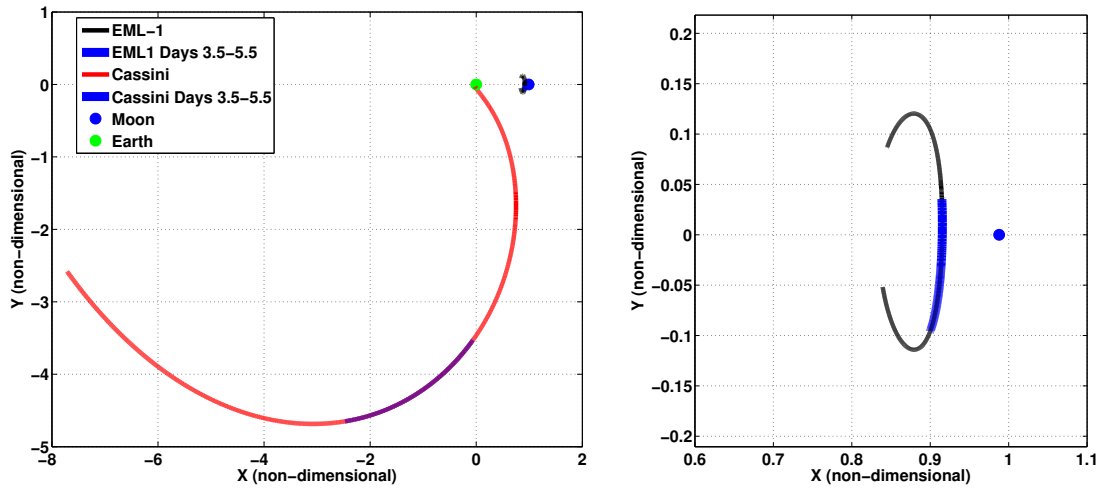


Figure 14: Geometry of the Cassini spacecraft shown highlighting days 3.5 through 5.5 (shown in blue) that led to poor geometry for LiAISON navigation. The full simulation is shown on the left, while the EML-1 satellite is shown close-up on the right.

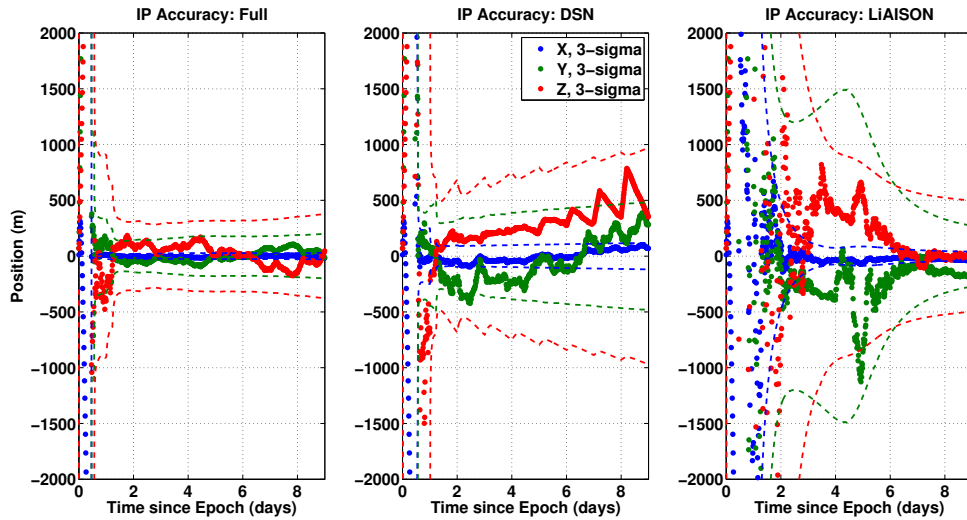


Figure 15: Interplanetary satellite position accuracies (truth - estimated) and 3-sigma uncertainty envelopes for the full (left), DSN-only (middle), and LiAISON-only (right) MER A mission simulations where the EML-1 satellite state is considered known and not estimated.

moves toward steady state throughout the 9 day measurement arc. Finally, the full simulation gives the best performance as expected.

CONCLUSION

A new adaptation of the Linked Autonomous Interplanetary Satellite Orbit Navigation (LiAISON) architecture, one satellite orbiting the Earth-Moon L_1 point and one departing on an interplanetary trajectory, has been analyzed. This study explored using LiAISON to obtain accurate orbit determination solutions for both spacecraft. A high-fidelity simulation was created to test several means of tracking the interplanetary depart-

ing trajectory. First, the full simulation consisted of continuous range and range-rate observations tracking from both LiAISON and the Deep Space Network. Subsequently, variations of this simulation were analyzed under the same conditions for comparison. It was found that observations from a navigation satellite orbiting at the Earth-Moon L_1 point could be used to supplement ground-based measurements and improve tracking performance. Additionally, it was shown that the extent to which LiAISON observations were effective in improving state estimation performance was highly dependent on the situational geometry. The best geometry is given by widely varying relative motion between the spacecraft, thereby allowing satellite-to-satellite tracking to more effectively leverage the asymmetry in the dynamical fields which is believed to be the source of LiAISON's advantage.

Several avenues exist for further exploration of this concept. First, additional fidelity could be introduced both in the filter set-up and the measurement model. Additional parameters could be introduced into the state, such as coefficient of reflectivity, to facilitate dynamical model calibration, for each spacecraft and measurement bias. Further, one of the challenges of tracking interplanetary-traveling spacecraft is the large link distances that quickly develop. More accurately modeling degrading effects due to these distances would increase real-world applicability. Finally, investigating the use of two LiAISON spacecraft to track the outbound trajectory at different EML-points may offset shortcomings in the geometry that degraded SST performance.

The configuration and simulations studied in this paper represent realistic navigation scenarios. The fidelity has been increased using operational uncertainties and *a priori* state errors. Moreover, dynamical errors were introduced in the filter. Each of these modeling complications were overcome and accurate results were obtained for both the Earth-Moon L_1 and simulated Cassini, Mars Exploration Rover A, and Mars Science Laboratory satellites. This work has demonstrated the potential capability of LiAISON in achieving more accurate navigation solutions for spacecraft departing on interplanetary trajectories.

ACKNOWLEDGEMENTS

The authors would like to thank the JPL Center Innovation Fund (CIF) Program, sponsored by NASA Office of the Chief Technologist (OCT), which has supported this research.

The research presented in this paper has been partially carried out at the Jet Propulsion Laboratory, California Institute of Technology, under a contract with the National Aeronautics and Space Administration. Government sponsorship acknowledged.

REFERENCES

- [1] K. Hill, M. W. Lo, and G. H. Born, "Linked, Autonomous, Interplanetary Satellite Orbit Navigation (LiAISON)," *AAS/AIAA Astrodynamics Specialists Conference*, No. AAS 05-399, Lake Tahoe, California, August 7-11 2005.
- [2] T. J. Martin-Mur, D. S. Abraham, D. Berry, S. Bhaskaran, R. J. Cesarone, and L. Wood, "The JPL roadmap for Deep Space navigation," tech. rep., Jet Propulsion Laboratory, 4800 Oak Grove Dr., Pasadena, CA 91109, January 2006.
- [3] K. Hill, J. Parker, G. H. Born, and N. Demandante, "A Lunar L2 Navigation, Communication, and Gravity Mission," *AIAA/AAS Astrodynamics Specialist Conference (AIAA/AAS, ed.)*, No. AIAA 2006-6662, Keystone, Colorado, August 2006.
- [4] Y.-C. Liu and L. Liu, "Orbit Determination Using Satellite-to-Satellite Tracking Data," *Chinese Journal of Astronomy and Astrophysics*, Vol. 1, No. 3, 2001.
- [5] K. Hill, *Autonomous Navigation in Libration Point Orbits*. PhD thesis, University of Colorado, Boulder, University of Colorado, Boulder, Colorado, 2007.
- [6] J. Parker, R. Anderson, G. Born, K. Fujimoto, J. Leonard, and R. McGranaghan, "Navigation Between Geosynchronous and Lunar L1 Orbiters," *Proceedings of the AIAA/AAS Astrodynamics Specialist Conference held 13-16 August 2012, Minneapolis, Minnesota, Paper AAS*, Jet Propulsion Laboratory and University of Colorado at Boulder, AIAA, 2012.
- [7] J. Leonard, R. McGranaghan, K. Fujimoto, G. Born, J. Parker, and R. Anderson, "LiAISON-Supplemented Navigation for Geosynchronous and Lunar L1 Orbiters," *Proceedings of the AIAA/AAS Astrodynamics Specialist Conference held 13-16 August 2012, Minneapolis, Minnesota, Paper AAS*,

- Minneapolis, MN, University of Colorado at Boulder and Jet Propulsion Laboratory, AIAA, August 13-16 2012.
- [8] K. Fujimoto, J. Leonard, R. McGranaghan, J. Parker, R. Anderson, and G. Born, "Simulating the LiAISON Navigation Concept in a GEO + Earth-Moon Halo Constellation," *23rd International Symposium on Space Flight Dynamics*, Pasadena, California, October 29 - November 2 2012.
- [9] J. M. Leonard, J. S. Parker, R. L. Anderson, R. M. McGranaghan, K. Fujimoto, and G. H. Born, "Supporting Crewed Lunar Exploration with LiAISON Navigation," *In Proceedings of the 35th AAS Guidance and Control Conference* (AAS/AIAA, ed.), No. AAS 13-053, Breckenridge, Colorado, University of Colorado at Boulder and Jet Propulsion Laboratory, February 2013.
- [10] J. S. Parker, J. M. Leonard, K. Fujimoto, R. M. McGranaghan, G. H. Born, and R. L. Anderson, "Navigating a Crewed Lunar Vehicle Using LiAISON," *Proceedings of the 23rd AAS/AIAA Spaceflight Mechanics Meeting* (AAS/AIAA, ed.), No. 13-330, Kauai, Hawaii, University of Colorado at Boulder and Jet Propulsion Laboratory, February 10-14 2013.
- [11] S. Broschart, M. Chung, S. Hatch, J. Ma, T. Sweetser, S. Weinstein-Weiss, and V. Angelopoulos, "Preliminary Trajectory Design for the ARTEMIS Lunar Mission," *Advances in Astronautical Sciences*, Vol. 134, 2009.
- [12] D. Folta, M. Woodard, and D. Cosgrove, "Stationkeeping of the First Earth-Moon Libration Orbiters: The ARTEMIS Mission," *Proceedings of the 2011 AIAA/AAS Astrodynamics Specialist Conference*, 2011.
- [13] M. Woodard, D. Cosgrove, P. Morinelli, J. Marchese, B. Owens, and D. Folta, "Orbit Determination of Spacecraft in Earth-Moon L1 and L2 Libration Point Orbits," *Proceedings of the AIAA/AAS Astrodynamics Specialist Conference*, No. AAS 11-514, Girdwood, Alaska, July 31 - August 4 July 31 - August 4, 2011.
- [14] K. Hill and G. Born, "Autonomous Orbit Determination from Lunar Halo Orbits Using Crosslink Range," *Journal of Spacecraft and Rockets*, Vol. 45, May - June 2008, pp. 548 - 553.
- [15] E. Standish, "JPL Planetary and Lunar Ephemerides, DE405/LE405," Jet Propulsion Laboratory Interoffice Memorandum IOM 312F-98-048, Aug. 26 1998.
- [16] D. Hoffman, "A Set of C Utility Programs for Processing JPL Ephemeris Data," Johnson Space Center, 1998.
- [17] G. Born, B. Tapley, and B. Schutz, *Statistical Orbit Determination*. Elsevier Academic Press, 2004.
- [18] P. Prince and J. Dormand, "High order embedded Runge-Kutta formulae," *Journal of Computational and Applied Mathematics*, Vol. 7, March 1981, pp. 67-75.
- [19] K. Hill and B. Jones, "Turboprop Version 4.0," Colorado Center for Astrodynamics, May 2009.
- [20] D. Richardson and N. Cary, "A Uniformly Valid Solution for Motion about the Interior Libration Point of the Perturbed Elliptic-Restricted Problem," *AAS/AIAA Astrodynamics Specialists Conference* (AAS/AIAA, ed.), No. AAS 75-021, July 28-30 1975.
- [21] H. Pernicka and K. Howell, "Numerical Determination of Lissajous Trajectories in the Restricted Three-Body Problem," *AIAA and AAS Astrodynamics Conference*, Aug. 18-20 1986.
- [22] R. Wilson, "Derivation of Differential Correctors Used in GENESIS Mission Design," Tech. Rep. JPL IOM 312.I-03-002, Jet Propulsion Laboratory, California Institute of Technology, 2003.
- [23] T. Ely, M. Heyne, and J. Riedel, "Altair Navigation Performance During Translunar Cruise, Lunar Orbit, Descent, and Landing," *Journal of Spacecraft and Rockets*, Vol. 49, March-April 2012, pp. 295-317.
- [24] T.-H. You, P. Antreasian, S. Broschart, K. Criddle, E. Higa, D. Jefferson, E. Lau, S. Mohan, M. Ryne, and M. Keck, "Gravity Recovery and Interior Laboratory Mission (GRAIL) Orbit Determination," *Proceedings of the 23rd International Symposium on Space Flight Dynamics (ISSFD)*, Pasadena, California 91109-8099, 29 Oct - 2 Nov 2012.
- [25] F. Peralta and S. Flanagan, "Cassini Interplanetary Trajectory Design," tech. rep., Jet Propulsion Laboratory, 1995.
- [26] R. B. Roncoli and J. M. Ludwinski, "Mission Design Overview for the Mars Exploration Rover Mission," Tech. Rep. 2002-4823, American Institute of Aeronautics and Astronautics, Pasadena, California 91109-8099, 2002.
- [27] T. Martin-Mur, G. Kruizinga, P. Burkhart, M. Wong, and F. Abilleira, "Mars Science Laboratory Navigation Results," tech. rep., Jet Propulsion Laboratory, California Institute of Technology, 4800 Oak Grove Dr., Pasadena, CA 91109, 2012.